


# Investigating the Impact of Sensor Placement on the Stability of Power Hardware-in-the-Loop with a Grid-Following Inverter as Hardware-of-Interest

Fargah Ashrafidehkordi 

*Institute of Technical Physics (ITEP)*  
*Karlsruhe Institute of Technology (KIT)*  
Karlsruhe, Germany

Giovanni De Carne 

*Institute of Technical Physics (ITEP)*  
*Karlsruhe Institute of Technology (KIT)*  
Karlsruhe, Germany

**Abstract**—Power Hardware-in-the-Loop (PHIL) is a fidelitous and reliable testing approach to evaluate the integration of emerging power technologies such as renewable resources in the power grid. However, when integrating the hardware-of-interest (HoI) with an emulated grid, insufficient prior knowledge about the HoI and transfer latencies in a PHIL setup can lead to loop instability, potentially resulting in hardware damage. Therefore, analyzing the loop stability before performing experiments is crucial. This paper approaches the impedance-based method to analyze the stability of a PHIL when testing a three-phase grid-following inverter with an LCL filter. The contribution lies in examining the impact of current and voltage sensor placement on the PHIL stability in four different scenarios: two for current and the other two for voltage sensor within the LCL filter. The results are presented and validated through time and frequency responses using Simulink/MATLAB.

**Index Terms**—Power hardware-in-the-loop, impedance-based stability, grid-following inverter, sensor placement.

## I. INTRODUCTION

In a Power Hardware-in-the-Loop (PHIL) setup, a real-time simulator incorporating a grid model, known as Software-of-Interest (SoI), is combined with specific interfaces, e.g., amplifier to replicate a realistic grid environment on a laboratory scale. The interaction between a Hardware-of-Interest (HoI) and the emulated grid can be studied across diverse grid scenarios [1].

The literature demonstrates various applications of PHIL, including microgrid controller testing [2], renewable integration studies [3], and electric vehicle (EV) charging infrastructure [4]. However, in a typical PHIL setup, the real-time simulator introduces two time-step delays to emulate the grid, while interfaces such as sensors and power amplifier (depending on its bandwidth), may introduce additional phase shifts. These phase shifts contribute to inaccuracies compared to the actual grid. Moreover, increased delays in the system reduce stability margins. The primary objective of employing PHIL is to analyze the interaction between the HoI and the emulated grid, which is often unrecognized prior to a PHIL

experiment. The lack of prior knowledge about the HoI/SoI interaction and delays introduced by system components and interfaces threaten closed-loop stability and may lead to potential hardware damage. Therefore, ensuring setup stability in the preparatory phase of PHIL experiments is crucial to prevent hardware damage and ensure result accuracy.

Analyzing grid-connected inverters as HoI is increasingly common due to their wide-ranging applications [5] and [6]. The same as grid-tied inverter integration stability analysis [7], applying the impedance-based method for stability analysis in a PHIL setup eliminates the necessity for a detailed HoI/SoI model to guarantee system stability [8]. The impact of inverter controller bandwidth, numerical filter cut-off frequency, impedance shifting, selecting interface algorithm, and compensators on the stability of a PHIL is well-studied in the literature [9]–[11].

As highlighted in [12], the placement of sensors for controlling a grid-following inverter can vary across LCL filters for different applications, making four combinations:

- 1) Current sensor location on the grid side inductor
- 2) Current sensor location on the inverter side inductor
- 3) Voltage sensor location across the Point of Common Coupling (PCC)
- 4) Voltage sensor location across the capacitor of the LCL filter

Nevertheless, the repercussions of sensor placement on stability when tested in a PHIL setup remain unexplored.

This paper examines a comparative exploration of the stability of these four scenarios when a grid-following inverter is taken in HoI. Section II introduces the PHIL setup and each component's respective transfer function. The system is then modeled through two impedances: grid impedance, including the grid model, amplifier bandwidth, conversion delays, and numerical low-pass filter, and inverter impedance, including the current controller, delays, and LCL filter. The open-loop transfer function is derived using the impedance ratio. Section III focuses on verifying the impedances, comparing bode plots of the modeled impedances and harmonic measurements in the simulated system. Moving on to section IV, the stability condition is demonstrated by demonstrating the time-domain

This work was supported by the Helmholtz Association under the program “Energy System Design” and within the Helmholtz Young Investigator Group “Hybrid Networks” (VH-NG-1613).

response of the model implemented in Simulink and corresponding the Nyquist plots of the impedance ratio. Finally, the paper concludes by summarizing critical understandings drawn from the study.

## II. MODELING THE SELECTED PHIL SETUP

The voltage-type ideal transformer method (V-ITM), which employs the linear power amplifier functioning as a voltage source, is chosen as the interface algorithm. Illustrated in Fig. 1, the Thevenin equivalent of the grid is created using a voltage source in series with an RL impedance. The modeling process considers various delays, including digital real-time simulator (DRTS), D/A, A/D, sensor, power amplifier, and the amplifier's dynamics. Within the digital-real-time simulator (DRTS), a numerical low-pass filter is interfaced into the feedback loop to eliminate high-frequency measurement noise. The HoI in this study is a grid-following inverter with an LCL filter modeled as a dq-based current-controlled voltage source. Fig. 1 shows sensor placement scenarios. Altering the location of the current sensor means transitioning the controlled variable from  $i_g$  to  $i_i$ . Similarly, changing the voltage sensor impacts the feedforward, influencing the dynamics of the controlled variable. Establishing the stability criterion in this section involves deriving the open-loop transfer function for each scenario via impedance-based modeling.

### A. Case I: $V_g, i_g$

In this case, PCC variables are fed into the control unit; namely, the  $i_g$  is controlled, and  $V_g$  is feedforwarded. A similar approach as in [8] but with feedforward is adopted here. The system shown in Fig. 1 is modeled with two impedances and two sources at the sides of PCC through the following equations.

$$G_{ifw} = G_{Amp}G_{D/A}G_{SoI} \quad (1)$$

$$G_{Amp} = e^{-(T_{Amp})s} / ((1/\omega_0)s^2 + (2D/\omega_0)s + 1) \quad (2)$$

$$G_{D/A} = e^{-(T_{D/A})s} \quad (3)$$

$$G_{SoI} = e^{-(T_{SoI})s} \quad (4)$$

Where  $G_{Amp}$  is the transfer function of the linear amplifier with the cut-off frequency of  $\omega_0$ , damping factor of  $D$ , and the delay of  $T_{Amp}$ . Also, the delay of the D/A converter and real-time simulation delay are shown as  $T_{D/A}$  and  $T_{SoI}$ , respectively.

The feedback involves the delays of A/D and sensor and a first-order filter as an interface in the SoI to avoid numerical stability issues with the cut-off frequency of  $\omega_c$ , given as:

$$G_{ifb} = G_{Sensor}G_{A/D}G_{Filter} \quad (5)$$

$$G_{Sensor}(s) = e^{-(T_{Sensor})s} \quad (6)$$

$$G_{A/D}(s) = e^{-(T_{A/D})s} \quad (7)$$

$$G_{Filter}(s) = \omega_c / (s + \omega_c) \quad (8)$$

According to Fig. 1, the relation between  $V_g$  and  $i_g$  is given in (9):

$$V_g = (V_s + G_{ifb}Z_s i_g)G_{ifw} \quad (9)$$

$$Z_s = L_s s + R_s \quad (10)$$

The same as [8], by replacing the corresponding transfer functions given above in (9) and rearranging the equation, (11) is achieved, which describes the grid side of PCC with  $V_{grid}$  as a source, and  $Y_{grid}$  as the modeled admittance. It is to be noted that in this paper, the sign of  $V_{grid}$  is shown based on the direction of the current.

$$i_g = -\underbrace{\frac{1}{G_{ifb}Z_s}V_s}_{V_{grid}} + \underbrace{\frac{1}{G_{ifb}Z_s G_{ifw}}}_{Y_{grid}}V_g \quad (11)$$

Therefore, the impedance of the grid side becomes:

$$Z_{grid} = G_{SoI}G_{D/A}G_{Amp}G_{Sens}G_{D/A}G_{Filter}Z_s \quad (12)$$

For the inverter side, the relation between PCC variables is given as follows:

$$i_g = Y_1 V_i - Y_2 V_g \quad (13)$$

In which the  $i_g$  is the superposition of the current flowing by inverter,  $Y_1 V_i$  and that of by emulated grid,  $Y_2 V_g$ . Applying the superposition,  $Y_1$  and  $Y_2$  are calculated as:

$$Y_1 = Z_C / (Z_{L_g} Z_C + Z_C Z_{L_i} + Z_{L_i} Z_{L_g}) \quad (14)$$

$$Y_2 = (Z_C + Z_{L_i}) / (Z_{L_g} Z_C + Z_C Z_{L_i} + Z_{L_i} Z_{L_g}) \quad (15)$$

$$Z_{L_g} = L_g s + r_g \quad (16)$$

$$Z_{L_i} = L_i s + r_i \quad (17)$$

$$Z_C = 1 / (C_f s) + R_f \quad (18)$$

Where  $r_g$  and  $r_i$  are the internal resistors of the inductors. The relation between the voltage of the inverter's output and the PCC current can be shown through the current controller as in (19). The impact of PLL at impedance and, therefore, on the system's stability is ignored.

$$V_i = (i^* - T_d i_g)G_{PI}T_d + V_g T_d^2 \quad (19)$$

$$G_{PI} = k_p + k_i / s \quad (20)$$

$$T_d = e^{-(T_{dPI})s} \quad (21)$$

Where  $T_{dPI}$  is the delay of the controller. By replacing (19) to (13), the relation between  $i_g$  and  $V_g$ , for the inverter side is achieved as:

$$i_g = \underbrace{\frac{G_{PI}T_d Y_1}{1 + G_{PI}T_d^2 Y_1} i^*}_{i_{inv}} - \underbrace{\frac{Y_2 - Y_1 T_d^2}{1 + G_{PI}T_d^2 Y_1} V_g}_{Y_{inv}} \quad (22)$$

Which describes a current source,  $i_{inv}$ , and the inverter impedance model. Hence, the impedance of the inverter can be represented as:

$$Z_{inv} = -(1 + G_{PI}T_d^2 Y_1) / (Y_2 - Y_1 T_d^2) \quad (23)$$

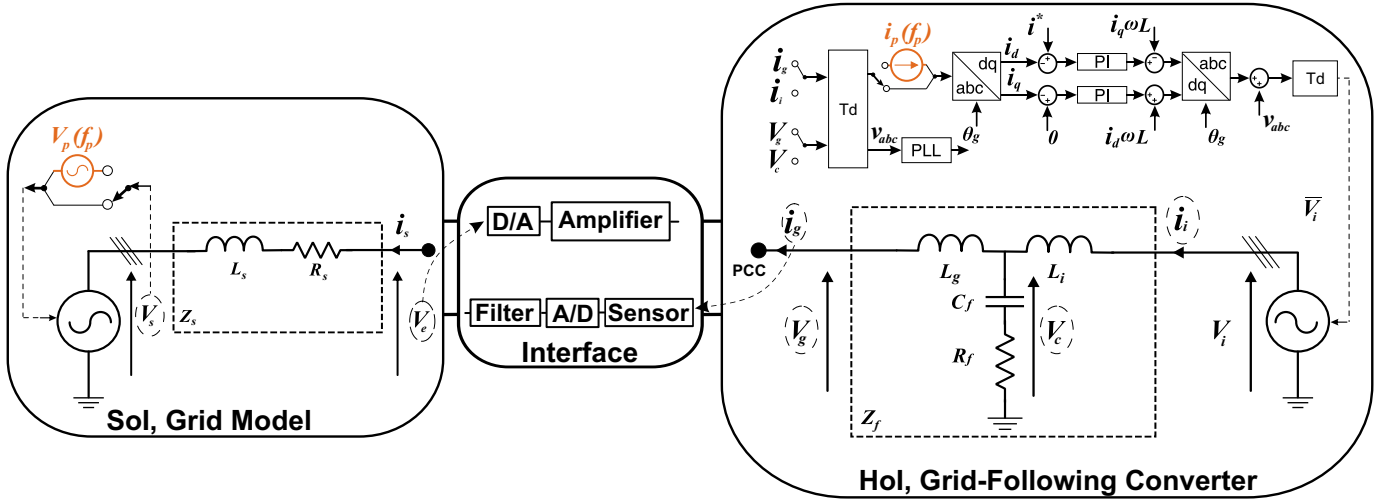


Fig. 1. Selected V-ITM PHIL setup: Cases I and II ( $i_g, i_i$ ) for the current sensors and Cases III and IV ( $V_g, V_c$ ) for the voltage sensors.  $V_p$  and  $i_p$  perturbation sources for impedance measurements serving the references for impedance verification

### B. Case II: $V_g, i_i$

The synchronization process occurs at the PCC, but now the control is shifted to the current on the inverter side. Alterations in sensor placements within the LCL filter mean the modeled grid impedance remains the same as in Case I across all the scenarios. Consequently, only the equations affected by these sensor placements are revised and provided here. Since the controlled variable is now the  $i_i$ , it is substituted to  $i_g$  in (19):

$$V_i = (i^* - T_d i_i) G_{PI} T_d + V_g T_d^2 \quad (24)$$

Where the same as Case I,  $i_i$  can be achieved by applying superposition:

$$i_i = Y_3 V_i - Y_1 V_g \quad (25)$$

$$Y_3 = (Z_C + Z_{L_g}) / (Z_{L_g} Z_C + Z_C Z_{L_i} + Z_{L_i} Z_{L_g}) \quad (26)$$

And  $i_g$  remains the same as in (13). Therefore, by replacing (25) to (24), and to (13), the inverter model is achieved as follows:

$$i_g = \underbrace{\frac{G_{PI} T_d Y_1}{1 + G_{PI} T_d^2 Y_3}}_{i_{inv}} i^* - \underbrace{\frac{Y_2 (1 + Y_3 G_{PI} T_d^2) - Y_1 T_d^2 (1 + Y_1 G_{PI})}{1 + G_{PI} T_d^2 Y_3}}_{Y_{inv}} V_g \quad (27)$$

The inverter impedance, as a result, becomes:

$$Z_{inv} = 1 / Y_{inv} \quad (28)$$

### C. Case III: $V_c, i_g$

Placing the voltage sensor at  $V_c$  means that synchronization and, consequently, feedforward is now over the capacitor of

the LCL filter. This means the relation between  $V_i$  and the controlled variable holds:

$$V_i = (i^* - T_d i_g) G_{PI} T_d + V_c T_d^2 \quad (29)$$

$$V_c = V_g + i_g Z_{L_g} \quad (30)$$

And by returning (30) to (29) and (29) to (13) the impedance model is achieved as following:

$$i_g = \underbrace{\frac{G_{PI} T_d Y_1}{1 + (G_{PI} - Z_{L_g}) T_d^2 Y_1}}_{i_{inv}} i^* - \underbrace{\frac{Y_2 - Y_1 T_d^2}{1 + (G_{PI} - Z_{L_g}) T_d^2 Y_1}}_{Y_{inv}} V_g \quad (31)$$

### D. Case IV: $V_c, i_i$

In the last scenario, the inverter side current is controlled, and the inverter is synchronized with the grid at the capacitor leg of the filter. Therefore:

$$V_i = (i^* - T_d i_i) G_{PI} T_d + V_c T_d^2 \quad (32)$$

By returning (25) and (30) to (32), and (32) to (25) the impedance model is achieved and shown below:

$$i_g = \underbrace{\frac{G_{PI} T_d Y_1}{1 + (Y_3 G_{PI} - Y_1 Z_{L_g}) T_d^2}}_{i_{inv}} i^* - \underbrace{\frac{Y_2 (1 + Y_3 G_{PI} T_d^2) - Y_1 T_d^2 (1 + G_{PI} Y_1)}{1 + (Y_3 G_{PI} - Y_1 Z_{L_g}) T_d^2}}_{Y_{inv}} V_g \quad (33)$$

With the setup now fully modeled, incorporating grid and inverter sources along with impedances across all scenarios, the veracity of the models is validated in the next section.

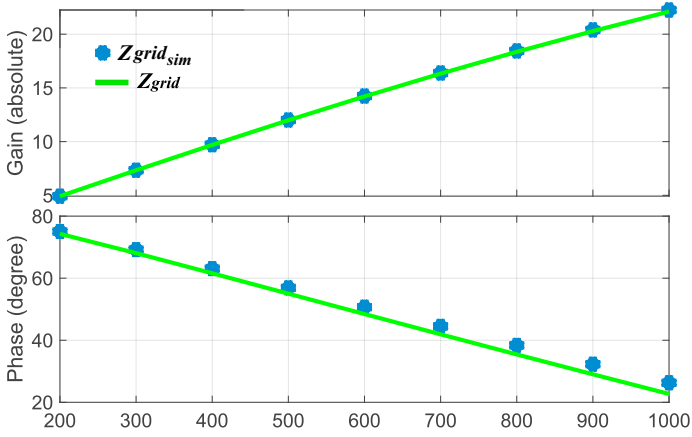


Fig. 2. Grid impedance verification

### III. IMPEDANCE VERIFICATION

To validate the impedance modeling, the setup shown in Fig. 1 is implemented in Simulink with the parameter given in Table I. The value of  $Z_s$  is set as 0.7 times the value of  $Z_{Lg}$ . Perturbations, shown in the figure as  $V_p$  and  $i_p$  in a range of 200-1000 Hz for  $f_p$  are applied. Then, PCC current and voltage are measured and fed to the Fourier transform for gain and phase measurements of  $Z_{inv_{ref}}$  and  $Z_{grid_{ref}}$ , respectively. The achieved values are compared with the Bode plot of modeled impedances in section II, and the comparison in each case is represented from Fig. 2 to 6. The proximity of the frequency response of the modeled impedances with measured values, as referenced, serves to validate the accuracy of the modeling approach.

A similar frequency response is apparent between cases I and II, as well as cases III and IV. In other words, the plots reveal minimal discrepancies in the gain and phase of inverter impedance when only the current sensor location is modified. However, a notable reduction in gain is observed when the voltage sensor is repositioned across the capacitor instead of PCC. Additionally, beyond 400 Hz, a gradual divergence in the phase of cases III and IV is observed, resulting in a distinct alteration in the shape of the inverter impedance compared to cases with  $V_g$ . With the model now validated in the preceding section, the stability of the system is to be assessed next via the impedance-based stability criterion.

### IV. STABILITY VERIFICATION

The stability of the system is affirmed based on the following stability criterion [7]:

$$G_{OL} = Z_{grid}/Z_{inv} \quad (34)$$

Where both impedances are modeled in the previous section. For verification, the  $C_f$  value is changed from 12 to 4  $\mu F$ . Then, the Nyquist plot of  $G_{OL}$  is illustrated along with the time response from the Simulink model in both cases. Similar to bode plots, Fig. 7 indicates that the response and stability margin in the first group of the first two cases are close to each other, the same as the second group. All cases with this

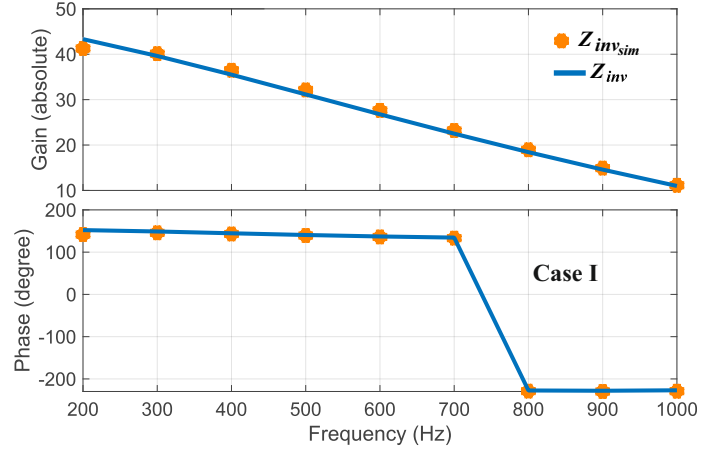


Fig. 3. Inverter impedance verification:  $V_g, i_g$

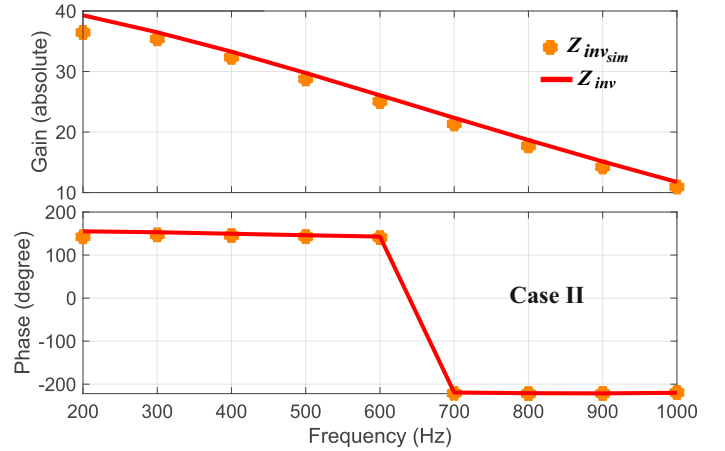


Fig. 4. Inverter impedance verification:  $V_g, i_c$

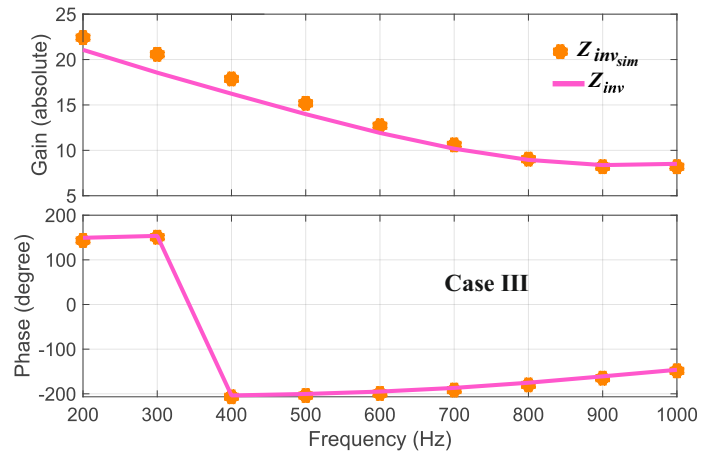


Fig. 5. Inverter impedance verification:  $V_c, i_g$

capacitor value are stable, and the margins of the all seem to be close. However, with a 4  $\mu F$ , as depicted in Fig 8, there is a margin difference between group one, namely cases I and II, which are unstable, and group two, cases III and

TABLE I  
PHIL SIMULATION PARAMETER

| $T_{SoI}$<br>[ $\mu s$ ] | $T_{Amp}$<br>[ $\mu s$ ] | $T_{A/D}, T_{D/A}$<br>[ $\mu s$ ] | $T_{Sensor}$<br>[ $\mu s$ ] | $T_{dPI}$<br>[ $\mu s$ ] | $\omega_0/(2\pi)$<br>[kHz] | $\omega_c/(2\pi)$<br>[kHz] | $L_s$<br>[mH] | $L_g$<br>[mH] | $L_i$<br>[mH] | $C_f$<br>[ $\mu F$ ] | $R_s$<br>[ $\Omega$ ] | $r_g, r_i$<br>[ $\Omega$ ] | $R_c$<br>[ $\Omega$ ] | $D$<br>— | $k_p$<br>— | $k_i$<br>— |
|--------------------------|--------------------------|-----------------------------------|-----------------------------|--------------------------|----------------------------|----------------------------|---------------|---------------|---------------|----------------------|-----------------------|----------------------------|-----------------------|----------|------------|------------|
| 50                       | 1.5                      | 3                                 | 3                           | 50                       | 180                        | 2                          | 3.37          | 2.36          | 2.36          | 12                   | 0.07                  | 0.05                       | 1                     | 0.9      | 1          | 40         |

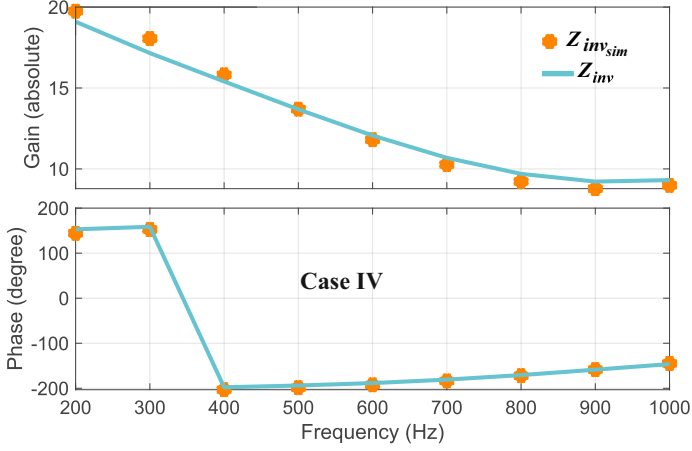


Fig. 6. Inverter impedance verification:  $V_c, i_c$

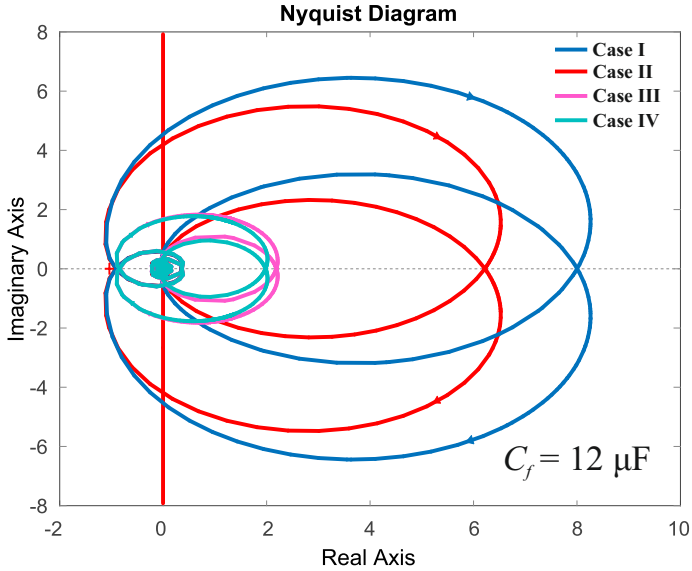


Fig. 7. Nyquist plot of  $Z_{grid}/Z_{inv}$ , all cases are stable

IV, which are within the stable zone. Based on Nyquist plots, when the voltage sensor is placed across the capacitor of the LCL filter, the stability of the system is enhanced, whereas the current sensor's location does not impact the closed-loop stability of such a system. To prove this finding, the time domain response from the implemented Simulink model is shown in Fig.9, where at 0.7 s, the voltage sensor is switched from the capacitor's location to the PCC (from  $V_c$  to  $V_g$ ), and the system becomes unstable and at 0.8 s, it is switched back to case III and the system regains the stability, confirming the

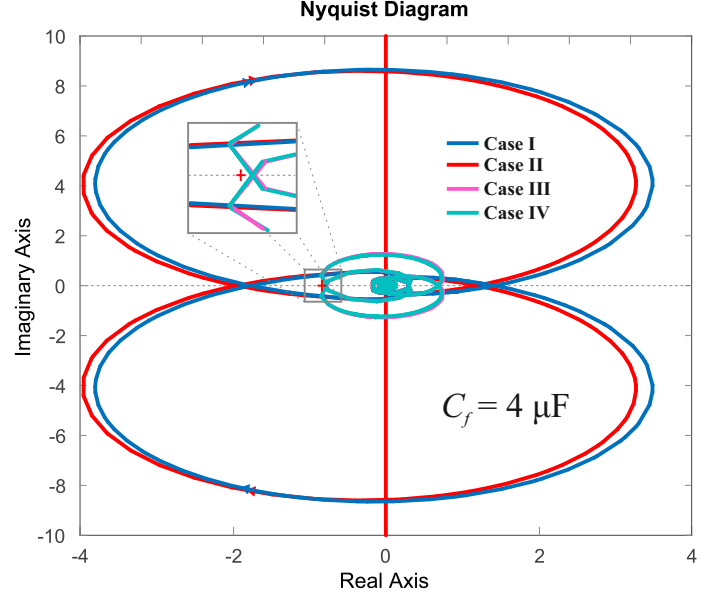


Fig. 8. Nyquist plot of  $Z_{grid}/Z_{inv}$ , case I and II are unstable, cases III and IV are stable

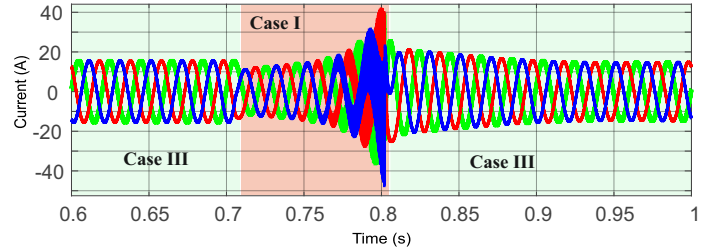


Fig. 9. Time domain response of the controlled current when changing the position of the voltage sensor

Nyquist plot's correctness.

## V. CONCLUSION

The positioning of voltage/current sensors in grid-connected scenarios can vary depending on specific applications. Understanding the impact of sensor positioning on system stability is crucial, specifically for Power Hardware-in-the-Loop (PHIL) users. This paper focuses on assessing the stability of a grid-following inverter with an LCL filter, serving as the hardware of interest, across four potential sensor placement combinations. The inverter impedance, influenced by sensor placement, is modeled analytically and verified via simulations for each case in Simulink. Then, through the Nyquist plots

of the impedance-based creation, the stability of all cases is assessed and verified with time domain simulations. The achievements derived from this study show that a change in the location of the voltage sensor can cause a notable impact on stability margin, while the change in the current sensor location appears negligible. Placing the voltage sensor over the capacitor enhances its stability compared to placing it on PCC. This conclusion can benefit PHIL users by balancing system stability according to the requirements of their respective test case applications.

#### REFERENCES

- [1] W. Ren, M. Steurer, and S. Woodruff, "Applying controller and power hardware-in-the-loop simulation in designing and prototyping apparatuses for future all electric ship," in *2007 IEEE Electric Ship Technologies Symposium*, 2007, pp. 443–448.
- [2] H. Kikusato, T. S. Ustun, M. Suzuki, S. Sugahara, J. Hashimoto, K. Otani, K. Shirakawa, R. Yabuki, K. Watanabe, and T. Shimizu, "Integrated power hardware-in-the-loop and lab testing for microgrid controller," in *2019 IEEE Innovative Smart Grid Technologies - Asia (ISGT Asia)*, 2019, pp. 2743–2747.
- [3] M. Steurer, F. Bogdan, W. Ren, M. Sloderbeck, and S. Woodruff, "Controller and power hardware-in-loop methods for accelerating renewable energy integration," in *2007 IEEE Power Engineering Society General Meeting*, 2007, pp. 1–4.
- [4] A. Mazza, E. Pons, E. Bompard, G. Benedetto, P. Tosco, M. Zampolli, and R. Jaboeuf, "A power hardware-in-the-loop laboratory setup to study the operation of bidirectional electric vehicles charging stations," in *2022 International Conference on Smart Energy Systems and Technologies (SEST)*, 2022, pp. 1–6.
- [5] P. Teske, M. Eggers, H. Yang, and S. Dieckerhoff, "Power Hardware-in-the-Loop Testbench for Grid-Following and Grid-Forming Inverter Prototyping," *2022 IEEE 13th International Symposium on Power Electronics for Distributed Generation Systems, PEDG 2022*, 2022.
- [6] T. Reinikka, H. Alenius, T. Roinila, and T. Messo, "Power hardware-in-the-loop setup for stability studies of grid-connected power converters," in *2018 International Power Electronics Conference (IPEC-Niigata 2018 -ECCE Asia)*, 2018, pp. 1704–1710.
- [7] J. Sun, "Impedance-based stability criterion for grid-connected inverters," *IEEE Transactions on Power Electronics*, vol. 26, no. 11, pp. 3075–3078, 2011.
- [8] F. Ashrafiidehkordi, X. Liu, and G. De Carne, "Impedance-based Stability Analysis of a Power Hardware-in-the-Loop for Grid-Following Inverter Testing." Nashville: ECCE, 10 2023.
- [9] W. Ren, M. Steurer, and T. L. Baldwin, "Improve the Stability and the Accuracy of Power Hardware-in-the-Loop Simulation by Selecting Appropriate Interface Algorithms," in *2007 IEEE/IAS Industrial & Commercial Power Systems Technical Conference*. IEEE, 5 2007, pp. 1–7.
- [10] B. Lundstrom and M. V. Salapaka, "Optimal Power Hardware-in-the-Loop Interfacing: Applying Modern Control for Design and Verification of High-Accuracy Interfaces," *IEEE Transactions on Industrial Electronics*, vol. 68, no. 11, pp. 10 388–10 399, 11 2021.
- [11] A. Paspatis, A. Kontou, Z. Feng, M. Syed, G. Lauss, G. Burt, P. Kotsamopoulos, and N. Hatzigryriou, "Virtual Shifting Impedance Method for Extended Range High-Fidelity PHIL Testing," *IEEE Transactions on Industrial Electronics*, vol. 71, no. 3, pp. 2903–2913, 3 2024.
- [12] R. Teodorescu, M. Liserre, and P. Rodriguez, *Grid Converters for Photovoltaic and Wind Power Systems*. Wiley, 2010.